Evolution of competing magnetic order in the $J_{\text{eff}} = 1/2$ insulating state of $Sr_2Ir_{1-x}Ru_xO_4$

S. Calder,[1,*] J. W. Kim,[2] G.-X. Cao,[3,4] C. Cantoni,[4] A. F. May,[4] H. B. Cao,[1] A. A. Aczel,[1] M. Matsuda,[1] Y. Choi,[2] D. Haskel,[2] B. C. Sales,[4] D. Mandrus,[3,4] M. D. Lumsden,[1] and A. D. Christianson[1,5]

[1]*Quantum Condensed Matter Division, Oak Ridge National Laboratory, Oak Ridge, Tennessee 37831, USA*

[2]*Advanced Photon Source, Argonne National Laboratory, Argonne, Illinois 60439, USA*

[3]*Department of Materials Science and Engineering, University of Tennessee, Knoxville, Tennessee 37996, USA*

[4]*Materials Science and Technology Division, Oak Ridge National Laboratory, Oak Ridge, Tennessee 37831, USA*

[5]*Department of Physics and Astronomy, University of Tennessee, Knoxville, Tennessee 37996, USA*

(Received 7 August 2015; published 27 October 2015)

We investigate the magnetic properties of the series $Sr_2Ir_{1-x}Ru_xO_4$ with neutron, resonant x-ray, and magnetization measurements. The results indicate an evolution and coexistence of magnetic structures via a spin-flop transition from *ab*-plane to *c*-axis collinear order as the $5d$ Ir^{4+} ions are replaced with an increasing concentration of $4d$ Ru^{4+} ions. The magnetic structures within the ordered regime of the phase diagram ($x < 0.3$) are reported. Despite the changes in magnetic structure no alteration of the $J_{\text{eff}} = 1/2$ ground state is observed. The behavior of $Sr_2Ir_{1-x}Ru_xO_4$ is consistent with electronic phase separation and diverges from a standard scenario of hole doping. The role of lattice alterations with doping on the magnetic and insulating behavior is considered. The results presented here provide insight into the magnetic insulating states in strong spin-orbit coupled materials and the role perturbations play in altering the behavior.

DOI: 10.1103/PhysRevB.92.165128 PACS number(s): 75.70.Tj, 78.70.Nx, 71.20.Ps, 71.20.Be

I. INTRODUCTION

Investigations of materials with $5d$ transition metal ions have opened up new paradigms in condensed-matter physics. In this regime spin-orbit coupling (SOC) can play a prominent role by competing directly with several phenomena, such as electron correlations, lattice alterations, bandwidth, and crystal-field splitting [1]. The consequence of these finely balanced interactions is diverse behavior and allows $5d$ systems to span a wide phase space containing metals and insulators with exotic behavior such as Weyl semimetals, axion insulators, and metal-insulator transitions [1–3]. Moreover robust magnetism often emerges, despite the apparent obstacle of reduced correlation and itinerant nature of $5d$ ions compared to analogous $3d$ based systems.

Particular focus in $5d$ systems with strong SOC has centered on iridates containing Ir^{4+} ions [1]. These systems can host unusual magnetic insulating states where the SOC splits the nondegenerate $5d^5 t_{2g}$-manifold into a fully occupied $J_{\text{eff}} = 3/2$ manifold and a half-filled $J_{\text{eff}} = 1/2$ shell that can be further split by the on-site Coulomb interaction. The result is a magnetic $J_{\text{eff}} = 1/2$ SOC Mott-like insulating state. Experimental evidence was initially reported in Sr_2IrO_4 [4], followed by an increasing number of Ir^{4+} based transition metal oxides [5–9].

The role of magnetism and lattice effects, notably the existence of the $J_{\text{eff}} = 1/2$ state despite significant noncubic distortions, have continued to prompt debate as to the nature of the ground state and subsequent emergent properties. In this investigation we perturb Sr_2IrO_4 via chemical substitution. Both electron doping and hole doping Sr_2IrO_4 are interesting avenues that have undergone limited investigations. Indeed superconductivity has been postulated to occur via electron doping on the Sr site [10] and experimental evidence of the proximity of the parent compound to a superconducting regime has been proposed due to analogous spin excitations with the parent cuprates [11]. Conversely hole or electron doping on the Ir site offers a handle to control the on-site and intrasite interactions of the magnetic ion responsible for the $J_{\text{eff}} = 1/2$ state. In this investigation we follow the latter route and investigate the series $Sr_2Ir_{1-x}Ru_xO_4$ over the full magnetically ordered regime and into the unordered state. We verify that this corresponds to hole doping with the substitution of $4d^4$ Ru^{4+} ions on the $5d^5$ Ir^{4+} site. A key focus of our investigation is the magnetism in the strong SOC limit. In this regime interesting physics can emerge due to SOC allowing the mixing of orbitals, where symmetry would usually prohibit such an occurrence. This can lead to the presence of dominant anisotropic rather than isotropic magnetic exchange couplings in the ground state in the form of Kitaev interactions [12].

The end members of the $Sr_2Ir_{1-x}Ru_xO_4$ series exhibit distinct physical behavior. Sr_2RuO_4 is a nearly ferromagnetic metal which exhibits unconventional superconductivity below 1.5 K attributed to *p*-wave pairing [13]. The electronic configuration of the Ru^{4+} ion results in $S = 1$ in contrast to the $J_{\text{eff}} = 1/2$ antiferromagnetic insulating state in Sr_2IrO_4. Therefore Sr_2RuO_4 (metallic) and Sr_2IrO_4 (insulator) reside on opposite sides of a metal-insulator divide. Both Sr_2RuO_4 and Sr_2IrO_4 form the K_2NiF_4-type structure, with Sr_2RuO_4 adopting the $I4/mmm$ space group and Sr_2IrO_4 the $I4_1/acd$, although a recent report suggested the $I4_1/a$ space group [14]. The difference between the space groups for Sr_2IrO_4 and Sr_2RuO_4 is the result of rotation of the IrO_6 octahedra. This series was previously investigated in Ref. [15], where x-ray diffraction indicated the structural change for the series $Sr_2Ir_{1-x}Ru_xO_4$ to occur around $x = 0.7$. That investigation was restricted to powder samples and involved no microscopic probes of magnetism. Recently a Raman investigation measured single crystals of $Sr_2Ir_{1-x}Ru_xO_4$, with the measurements focusing on the octahedral rotations [16]. Here we investigate single crystals with both neutron scattering and resonant magnetic

*caldersa@ornl.gov

x-ray scattering (RMXS) that allows us to probe the long-range magnetic structure and nature of the electronic ground state of the Ir ion as a function of Ru doping and consider the role of the competing interactions in the system.

II. EXPERIMENTAL METHODS

Single crystals of $Sr_2Ir_{1-x}Ru_xO_4$ were grown in a Pt crucible using the flux method. Crystals of mm dimensions with masses ranging 5–20 mg were produced for Ru concentrations up to 40%. Additionally powder samples of $x = 0.05$ and 0.2 were prepared by standard solid-state techniques. Neutron scattering was performed on the single crystals at the High Flux Isotope Reactor (HFIR) on HB-1, HB-1A, and HB-3A. The triple axis instrument HB-1A was used in elastic mode with a wavelength of 2.36 Å and collimation 40′-40′-open-open to determine the magnetic structure. Polarized neutron-scattering measurements were performed on HB-1. Heusler monochromator and analyzer crystals were used to perform the polarized measurements with a guide field giving the option of flipping the spin in horizontal and vertical fields at the sample position. The beam was collimated with 48′-open-80′-open solar collimators. The crystal structure was measured on the four-circle single-crystal neutron diffractometer HB-3A with a wavelength of 1.003 Å. Measurements on the powder samples were carried out on the HB-2A powder diffractometer at HFIR using a wavelength of 1.54 Å. Resonant magnetic x-ray scattering (RMXS) measurements were performed on beamline 6-ID-B at the Advanced Photon Source (APS) on single crystals. Measurements were carried out at both the L_2 (12.824 keV) and L_3 (11.215 keV) resonant edges of iridium. Graphite was used as the polarization analyzer at the (0 0 10) and (0 0 8) reflections on the L_2 and L_3 edges, respectively, to achieve a scattering angle close to 90°. An analysis of the photon polarization allowed magnetic and charge scattering to be distinguished. To observe the sample fluorescence, energy scans were performed without the analyzer and with the detector away from any Bragg peaks through both absorption energies. X-ray magnetic circular dichroism (XMCD) and x-ray-absorption near-edge spectroscopy (XANES) were performed at the Ir $L_{2,3}$ edge on beamline 4-ID-D at the APS. The XMCD measurements were performed in an ±3 T field at 1.8 K. Powder samples were used to ensure uniform sample thickness and all measurements were performed in transmission mode. The sample magnetization $M(T,H)$ was measured with a Quantum Design (QD) magnetic property measurement system (MPMS) with an applied field of 100 Oe.

III. RESULTS AND ANALYSIS

A. Valence determination of Ir in $Sr_2Ir_{1-x}Ru_xO_4$

We initially consider whether the introduction of Ru onto the Ir site alters the valence state of iridium. It is reasonable to assume that Ru adopts the Ru^{4+} valence resulting in $Sr_2Ir_{1-x}{}^{4+}Ru_x{}^{4+}O_4$ for all values of x. However, a similar reasoning proved incorrect in the series $Sr_2Ir_{1-x}Rh_xO_4$. There Rh formed Rh^{3+} for $x > 0$ resulting in mixed magnetic Ir^{4+} and nonmagnetic Ir^{5+} [17]. To probe the Ir valence in $Sr_2Ir_{1-x}Ru_xO_4$ we performed XANES measurements on the

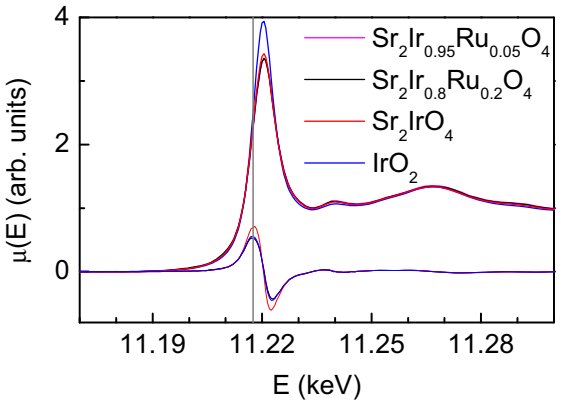

FIG. 1. (Color online) XANES measurements at the Ir L_3 edge for $Sr_2Ir_{1-x}Ru_xO_4$, with $x = 0$, 0.05, and 0.2, and a IrO_2 standard. The white line absorption intensity and the derivative are both shown for each sample. The same absorption energy of 11.2175 keV is observed for all the samples measured indicating a valence of Ir^{4+}.

$x = 0$, 0.05, and 0.2 members of the series and compared this to an established iridium standard IrO_2. The XANES results are shown in Fig. 1 and show no indication of an altered Ir valence from 4+, unlike similar measurements for the Rh case where a pronounced shift in the energy of the resonant edge was observed [17]. Results at the L_2 edge show a similar overlap in the energy position of the white line as the L_3 edge. Therefore the series $Sr_2Ir_{1-x}{}^{4+}Ru_x{}^{4+}O_4$ corresponds to hole doping on the Ir site.

B. Magnetization measurements of $Sr_2Ir_{1-x}Ru_xO_4$

We begin our magnetic investigation with magnetization measurements on single-crystal samples of $Sr_2Ir_{1-x}Ru_xO_4$ with $x = 0.05$, 0.1, 0.2, and 0.3, shown in Fig. 2. The results indicate a rather complicated magnetic temperature dependence with the $x = 0.05$ and $x = 0.1$ concentrations showing more than one anomaly. For example for $x = 0.05$

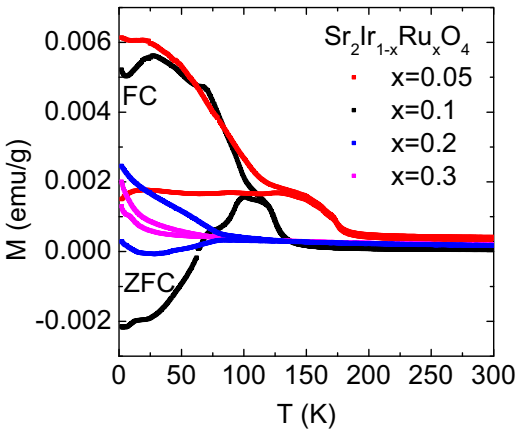

FIG. 2. (Color online) Magnetization measurements on single crystals in the series $Sr_2Ir_{1-x}Ru_xO_4$ for $x = 0.05$, 0.1, 0.2, and 0.3. Field-cooled (FC) and zero-field-cooled (ZFC) results in an applied field of 100 Oe are shown. The ZFC curve is always lower than the FC for all concentrations measured.

there are two pronounced anomalies, one around 200 K and another at 150 K. Similarly $x = 0.1$ has two anomalies, located at 125 and 160 K. The magnetization measurements in Fig. 2 indicate long-ranged magnetic order up to $x = 0.2$. At least qualitatively the results are similar to those on powder samples presented in Ref. [15] and therefore allow comparisons between our current investigation and the results previously obtained.

C. Magnetic structure of the series $Sr_2Ir_{1-x}Ru_xO_4$

To probe the magnetic structure we combine neutron and RMXS measurements. Results for RMXS measurements at the iridium L_3 edge are shown in Figs. 3(a) and 3(b) for $Sr_2Ir_{1-x}Ru_xO_4$ single crystals with concentrations of $x = 0.05$, 0.1, and 0.2. Magnetic scattering is observed at both $(1,0,2n)$ and $(1,0,2n+1)$ reflections for $x = 0.05$. Substituting in $x = 0.1$ produces the same magnetic reflections at $(1,0,2n)$ and $(1,0,2n+1)$, however the intensity of the $L =$ even reflections are much reduced compared to the $L =$ odd reflections. Moving to $x = 0.2$ only the $(1,0,2n+1)$ magnetic reflections are present.

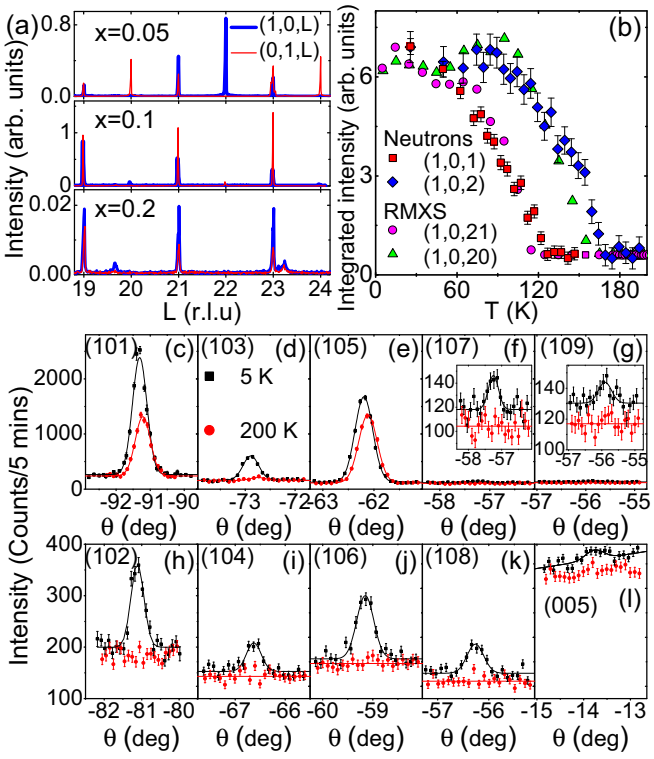

FIG. 3. (Color online) (a) RMXS measurements on single crystals of $Sr_2Ir_{1-x}Ru_xO_4$ with $x = 0.05$, 0.1, and 0.2. (b) Comparison of the intensity of $(1,0,2n+1)$ and $(1,0,2n)$ magnetic reflections in $Sr_2Ir_{0.9}Ru_{0.1}O_4$ measured with both neutrons and RMXS. The neutron and x-ray measurements involved different crystals from the same batch. The intensities have been normalized to their respective backgrounds intensities and scaled so all reflections are in a single plot. (c)–(l) Neutron-scattering rocking scan measurements on a single crystal of $Sr_2Ir_{0.9}Ru_{0.1}O_4$ for several reflections. Scattering is observed at $(1,0,L)$ for both $L =$ odd and $L =$ even.

This behavior diverges from the few previous cases where the magnetic structure has been probed in doped Sr_2IrO_4. Undoped Sr_2IrO_4 has magnetic $(1,0,2n)$ reflections with spins in the ab plane [4,18,19]. For Mn doping [20], Rh doping [17], or the application of an applied field [4] to Sr_2IrO_4, only $(1,0,2n+1)$ reflections are present, indicating an altered magnetic structure to the undoped case.

1. *Magnetic structure of* $Sr_2Ir_{0.9}Ru_{0.1}O_4$

Focusing on the $Sr_2Ir_{1-x}Ru_xO_4$ composition with $x = 0.1$ that has both $(1,0,2n)$ and $(1,0,2n+1)$ reflections we measured several Bragg peaks with neutrons and RMXS; see Fig. 3. Following specific reflections we find the magnetic order parameters reveal two distinct magnetic ordering temperatures; see Fig. 3(b). This is confirmed using both RMXS and neutrons on different samples. The $(1,0,2n+1)$ reflections develop at 120 K, whereas $(1,0,2n)$ reflections appear at 160 K. The ordering of the $(1,0,2n+1)$ reflections appear to not be reflected by any associated anomaly in the $(1,0,2n)$ order parameter, suggesting a possible decoupling or coexistence of two magnetic phases within the sample. Susceptibility measurements confirm a change in magnetization at these temperatures for $Sr_2Ir_{0.9}Ru_{0.1}O_4$ on a crystal from the same batch (Fig. 2), supporting the magnetic origin.

In order to gain further understanding of the long-range magnetic order in $Sr_2Ir_{0.9}Ru_{0.1}O_4$ we consider the polarization dependence of the scattering cross section, first with x rays and then with neutrons. A standard configuration to measure RMXS in is a vertical geometry, however by measuring in a horizontal geometry we can utilize the polarization dependence of the incoming beam and analyzed beam to determine the spin direction of the ordered moments within the sample; see Figs. 4(a) and 4(b). With the incoming beam π polarized we find intensity for π-π polarized analysis at the (0,3,1), equivalent to $(1,0,2n+1)$ reflection, and no intensity for π-σ

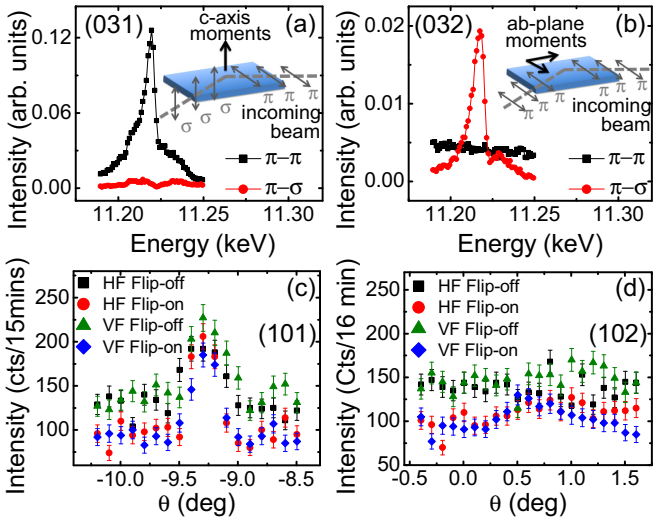

FIG. 4. (Color online) By performing polarization analysis of (a) and (b) x-ray energy scans and (c) and (d) neutron rocking scans on $Sr_2Ir_{0.9}Ru_{0.1}O_4$ single crystals, the spin direction associated with the magnetic reflections is determined. Both measurements were performed at 5 K.

polarization. This is consistent with spins oriented along the c axis in the sample. Conversely for the $(1,0,2n)$ reflection, measured at $(0,3,2)$, we observe the opposite behavior with intensity only at π-σ polarization that indicates the spins contributing to this reflection are confined to the ab plane. This behavior was confirmed with polarized neutron-scattering measurements on a single-crystal sample of $Sr_2Ir_{0.9}Ru_{0.1}O_4$ at the (101) and (102) reflections. For the (101) reflections intensity is observed in all the four channels measured from the combinations of horizontal field (HF), vertical field (VF), and flip on and flip off; see Fig. 4(c). This is consistent with both magnetic and nuclear contributions to the scattering, as expected given the observation of nuclear scattering at the (1 0 odd) reflections in the parent compound. Moreover with the crystal aligned in the $(H0L)$ plane it indicates c-axis oriented spins since the purely magnetic intensity (HF flip on) is similar to the magnetic intensity from the magnetic component perpendicular to the [101] direction in the $(H0L)$ scattering plane (VF flip on), which is almost along the c axis. Conversely the behavior of the (102) reflection is distinctly different, as shown in Fig. 4(d). The purely magnetic intensity (HF flip on), though reduced, is roughly similar to the magnetic intensity mostly from the magnetic component along the b axis (VF, flip off), in line with the conclusions from the RMXS results.

Following a representational analysis approach, there is no single magnetic structure consistent with a combination of both $(1,0,2n+1)$ and $(1,0,2n)$ reflections. We therefore considered the possibility of structural phase separation as an explanation for the apparent result of two coexisting sets of magnetic reflections. We carefully measured the 2θ dependence with both neutrons and x rays of several reflections and within the resolution found only one reflection; see Figs. 5(a) and 5(b) for representative plots. This is consistent with a single structural domain in the single-crystal samples studied here. This is based on the assumption that the two structural phases are epitaxial and would be accessible in the specific orientation of the aligned crystal. While this is a reasonable assumption given that the magnetic reflections are commensurate with the lattice we considered the phase separation scenario with further dedicated measurements.

To investigate the chemical homogeneity of the doped crystals at the nanoscale we employed aberration-corrected scanning transmission electron microscopy (STEM) and electron energy-loss spectroscopy (EELS). We imaged both doped and undoped samples using the high angle annual dark-field detector (HAADF), which yield images with an intensity (brightness) roughly proportional to Z^2 where Z is the element atomic number. In these images brighter (dimmer) spots represent heavier (lighter) columns, and oxygen columns are invisible due to their low Z. This technique also known as Z-contrast STEM or Z-STEM also yields a clear mass contrast: thicker sample regions appear brighter than thinner sample regions. This is evident in Figs. 5(c) and 5(e), in which the decreasing brightness from left to right is due to the decreasing thickness as the sample edge is approached (the vacuum appears black). Figures 5(c) and 5(d) and Figs. 5(e) and 5(f) are HAADF images of Sr_2IrO_4 and $Sr_2Ir_{0.9}Ru_{0.1}O_4$ samples, respectively, taken with the electron beam parallel to the [201] crystal axis. In this projection each spot represents

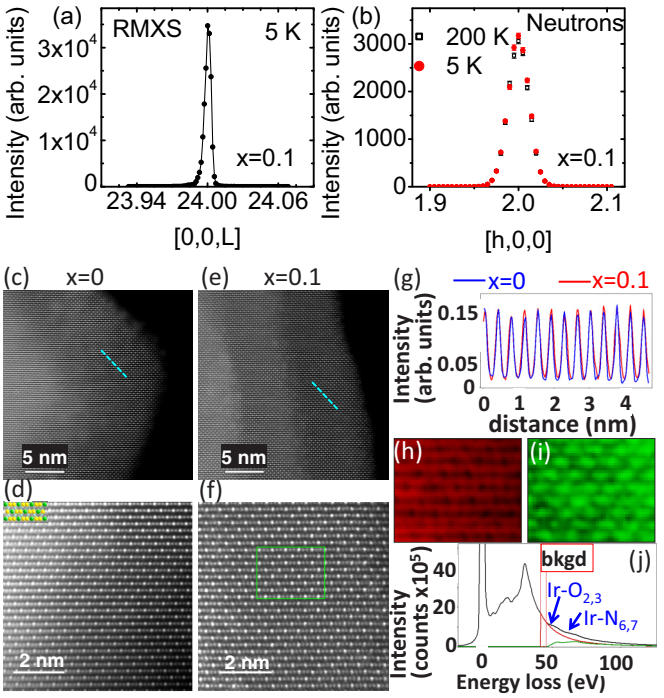

FIG. 5. (Color online) (a) Single-crystal synchrotron x-ray-diffraction measurements of $Sr_2Ir_{0.9}Ru_{0.1}O_4$ indicated no splitting of diffraction peaks, consistent with a homogeneous sample. (b) Neutron diffraction additionally found no evidence for structural phase separation. (c)–(j) High-resolution Z-STEM analysis of $Sr_2Ir_{1-x}Ru_xO_4$ samples. (c),(d) Z-contrast images of Sr_2IrO_4 at different magnifications with the beam parallel to [201]. Inset in (d) is a schematic model of the crystal with the Ir columns in green, the Sr columns in yellow, and the O columns (not imaged) in cyan. (e),(f) Z-contrast images of $Sr_2Ir_{0.9}Ru_{0.1}O_4$ with the same zone axis and the same magnification as in (c) and (d). (g) Line profile along the cyan segments in (c) and (e), showing the intensity (proportional to Z^2) of the Ir columns in Sr_2IrO_4 and $Sr_2Ir_{0.9}Ru_{0.1}O_4$ samples. (h) Uniform thickness map and (i) Ir map of the region indicated with a green rectangle in (f). (j) Electron energy-loss spectrum from the region within the green rectangle in (f) showing the Ir edges used to generate the Ir map by plotting their combined integrated intensity. The red curve is a power-law background fitting function and the green curve shows the background-removed Ir edges.

an atomic column containing only one type of element, either Sr or Ir, with a fraction of a Ru atom depending on the actual sample thickness. The uniformity of the images contrast within terraces of the same thickness and the similarity between the images for the undoped and doped samples suggest a uniform distribution of Ru dopants. In fact, given the large difference in the atomic masses of Ru and Ir, clustering of Ru dopants would likely give rise to lower intensity spots within a brighter matrix. If we probe the intensity of the Ir columns (the brighter spots) by taking a line profile in a small region of uniform thickness, as indicated by the cyan segment in Figs. 5(e) and 5(f), we find [see Fig. 5(g)] that the variation of this intensity is comparable in the parent and the doped samples, further indication that the Ru dopants are uniformly distributed [21]. In addition, we acquired an EELS spectrum image in the region indicated by the green rectangle in Fig. 5(f). Figure 5(h) shows

the thickness map of this region calculated using the EELS log-ratio method [22], and Fig. 5(i) shows the Ir elemental map obtained by plotting the integrated intensity of the Ir-$O_{2,3}$ and Ir-$N_{6,7}$ edges indicated in the EELS spectrum of Fig. 5(j) after background subtraction. We find that both the thickness distribution of the Ir columns and the distribution of the Ir columns' intensities in the Ir map show a standard deviation of only 1%, indicating very good doping homogeneity even down to the atomic scale.

Using a representational analysis approach to find the long-ranged-ordered magnetic structure from our neutron results for $Sr_2Ir_{0.9}Ru_{0.1}O_4$ [Figs. 3(c)–3(l)], we analyze the L = odd and L = even reflections separately. The experimental (1 0 even) reflections intensity for $L = 2,4,6,8$ is shown in Fig. 6(a), normalized to the (1,0,2) intensity. The results are qualitatively the same as the Sr_2IrO_4 undoped case presented by both Refs. [18,19]. To confirm this we modeled the magnetic structure, taking into account the Lorentz factor correction using ResLib [23], absorption of the sample, and magnetic form factor for Ir^{4+} using the information in Ref. [24]. The experimental and calculated results are shown in Fig. 6(a), along with the corresponding magnetic spin structure in Fig. 6(b). Close agreement is found between the experimental and calculated magnetic intensities indicating that this indeed corresponds to the magnetic ordering that results in the (1 0 even) reflections. In terms of representational analysis this corresponds to Γ_1, with a propagation vector $k = (111)$, for the Ir ion at the (0.5,0.25,0.125) position. Turning now to the (1 0 odd) reflections and following the polarization dependence that indicates c-axis aligned spins we model the magnetic structure. The experimental and calculated results are shown in Fig. 6(a) for $L = 1,3,5,7,9$. This corresponds to the Γ_1 irreducible representation, with a propagation vector $k = (000)$, for the Ir ion at the (0.5,0.25,0.125) position, as found for the case of Mn-doped Sr_2IrO_4 [20]. Again close agreement is found between the intensity of the experimental and calculated magnetic reflections.

Both magnetic structures, see Fig. 6(b), are related by a spin flop from the ab plane to the c axis. Given the apparent occurrence of these two competing magnetic structures and no evidence for structural phase separation we assign the behavior as being due to electronic phase separation. This conclusion is in line with that arrived at from the Raman investigation of $Sr_2Ir_{1-x}Ru_xO_4$ [16] and also the Ru doping behavior in the related iridate $Sr_3Ir_2O_7$ [25]. We note, however, the intriguing similarity of the magnetic structure to the ortho-G-AF phase presented in Ref. [26] that emerges from the Kugel-Khomskii model. For such a magnetic phase to exist would require weak nearest-neighbor interactions and appreciable second- and third-neighbor interactions and it remains unclear if such a phase would exist in this SOC dominated system [12].

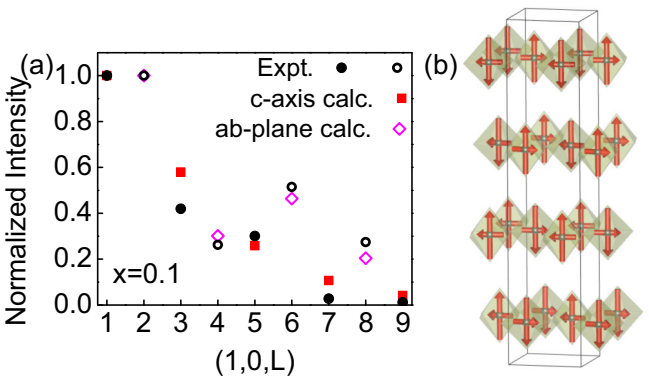

FIG. 6. (Color online) (a) Experimental neutron-scattering intensities for the magnetic reflections in $Sr_2Ir_{0.9}Ru_{0.1}O_4$ are compared with calculated magnetic structures for the case of spins in the ab plane and c axis. (b) Corresponding magnetic structures within the nuclear unit cell.

2. *Magnetic structure of* $Sr_2Ir_{0.8}Ru_{0.2}O_4$

Substituting in more Ru leads to the occurrence of only one magnetic transition for $Sr_2Ir_{0.8}Ru_{0.2}O_4$ at $T_N = 76.3(6)$ K; see Fig. 7(a). We measured the (101), (103), (105), and (107) reflections and obtained the intensities shown in Fig. 7(b). We again note that an additional weak nuclear contribution is present at (1 0 odd) reflections. Following the same method as for the (1 0 odd) case for the 10% Ru substitution we modeled the magnetic structure with spins along the c axis; this structure is shown in Fig. 7(c). The experimental and calculated intensities are compared in Fig. 7(b) and show close agreement. The ordered magnetic moment on the Ir ion is determined by scaling the magnetic intensities with measured nuclear reflections intensities. The ordered magnetic moment is $0.13(2)\mu_B$/Ir. Going to higher concentrations of $Sr_2Ir_{0.7}Ru_{0.3}O_4$ no long-ranged magnetic order is observed.

D. Insulating state in $Sr_2Ir_{1-x}Ru_xO_4$

We now turn to consider the nature of the insulating state within the magnetically ordered regime. One of the

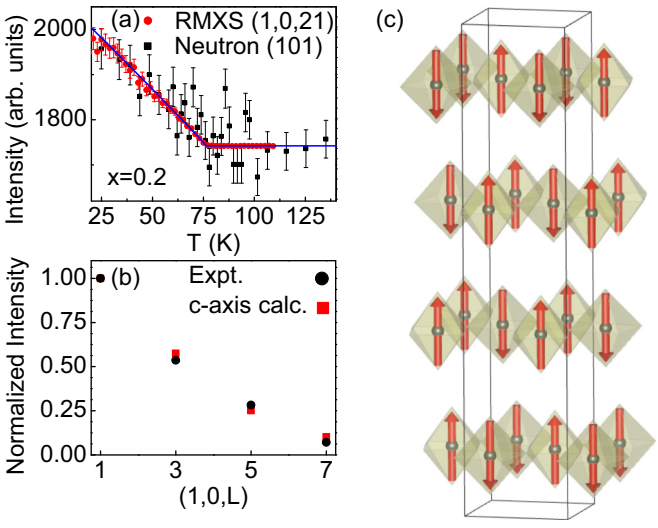

FIG. 7. (Color online) (a) Intensity dependence of the (1 0 odd) magnetic reflection measured with neutrons at (101) and RMXS at (1,0,21) for $Sr_2Ir_{0.8}Ru_{0.2}O_4$. The RMXS results are fit to a power law and give a transition temperature at $T_N = 76.3(6)$. (b) Experimental intensities for magnetic reflections compared to the calculated intensities for c-axis aligned spins. (c) The magnetic structure for $Sr_2Ir_{0.8}Ru_{0.2}O_4$ with spins aligned along the c axis.

principle experimental proofs of the SOC driven $J_{\text{eff}} = 1/2$ Mott insulating state in Sr_2IrO_4 was proposed on the basis of RMXS measurements [4]. It was argued that the observation of the large intensity at the L_3 and vanishing intensity at the L_2 edge was due to the alteration of the electronic ground state from a $S = 1/2$ to a $J_{\text{eff}} = 1/2$ scenario on the basis of the different $2p$-$5d$ transitions that are involved in the two different L edges probed with RMXS. Subsequently several investigations have proceeded along the same route and used the $L2 : L3$ branching ratio as evidence for a $J_{\text{eff}} = 1/2$ state. However, it has been argued that for the case of spins in the ab plane in the Sr_2IrO_4 structure vanishing intensity is expected at the L_2 regardless of whether the insulating state emerges from a $S = 1/2$ or $J_{\text{eff}} = 1/2$ ground state [27]. While this adds further debate as to whether the $J_{\text{eff}} = 1/2$ state exists in Sr_2IrO_4, we have shown that here the spins are, at least in certain Ru concentrations and temperature regions, aligned along the c axis. In this case the magnetic structure does not contribute to the suppression of intensity of the L edges; instead any suppression of intensity at the L_2 edge can be considered to be due to an alteration towards a $J_{\text{eff}} = 1/2$ ground state.

We therefore focus on the $(1,0,2n+1)$ reflections in $Sr_2Ir_{1-x}Ru_xO_4$ for $x = 0.1$ and 0.2. The results at the (1 0 21) magnetic Bragg reflection at 5 K are shown in Figs. 8(a) and 8(b). At the L_3 edge we observe a large enhancement for both $Sr_2Ir_{0.9}Ru_{0.1}O_4$ and $Sr_2Ir_{0.8}Ru_{0.2}O_4$ in the σ-π measurements, as expected for magnetic scattering. The maximum, as required, occurs at the inflection point of the absorption edge at 11.215 keV. In contrast, the behavior at the L_2 edge shows weak intensity in the σ-π measurements, with only weak scattering positioned at the absorption edge. The fluorescence measurement presented indicates the energy of the resonant edge only. This result therefore indicates that the SOC driven $J_{\text{eff}} = 1/2$ Mott insulating state exists within all of the magnetically ordered regimes of $Sr_2Ir_{1-x}Ru_xO_4$. This indicates that in general the $J_{\text{eff}} = 1/2$ state can host a variety of structures and interactions.

To provide further evidence that the L-edge branching ratio is indeed a valid measurement of the existence of a $J_{\text{eff}} = 1/2$ state we performed XMCD and XAS measurements on powder samples of $x = 0.05$ (both ab-plane and c-axis ordering) and $x = 0.2$ (only c-axis aligned spins) concentrations; see Figs. 8(c) and 8(d). These measurements do not rely on measuring at a magnetic Bragg reflection so in the $x = 0.05$ it will probe a mixture of magnetic ordering whereas in $x = 0.2$ it will probe only the c-axis ordering. The XMCD results show a reduced measured intensity with decreasing Ir concentrations, as would be expected, and a suppression of the intensity at the L_2 edge. For a system with negligible SOC the statistical branching ratio of the $L_2 : L_3$ edges from XAS is 2. Here we find for both the $x = 0.05$ and $x = 0.2$ a branching ratio of $\sim$4, similar to previous measurements on undoped Sr_2IrO_4, indicating a $J_{\text{eff}} = 1/2$ ground state [28].

E. Structural dependence of $Sr_2Ir_{1-x}Ru_xO_4$

In the magnetically ordered region of the phase diagram ($x < 0.3$) there is no structural symmetry change. However by performing single-crystal neutron diffraction in the magnetically ordered regime we are able to follow the octahedral alterations, that are believed to be intimately entwined with the nature of the magnetic insulating state [12]. The change in the rotation in the ab plane, α, and the tetragonal distortion, $\Delta_{\text{Ir-O}}$, here defined as the c/a ratio of the two octahedral Ir-O bonds, are shown in Fig. 9. As expected the octahedral rotation angle decreases along the series as we approach the $I4/mmm$ phase where $\alpha = 0$. In the $J_{\text{eff}} = 1/2$ limit it has been argued that the magnetic spins directly follow the canting within the ab plane. This has been verified in Sr_2IrO_4 [29]. From neutron scattering the occurrence of the (0,0,odd) reflection indicates a canting of the spin in the ab plane. The presence of the (0,0,5) reflection in 10% Ru doping shows that this persists upon doping and the orientation of the spin is consistent with following the rotation of the octahedra. As well as the octahedral rotation change the tetragonal distortion due to an elongation along the c axis of the octahedra increases. The significance in this has been shown theoretically in Refs. [12,30] to be a route to a spin flop from a magnetic structure with spins in the ab plane to a c-axis

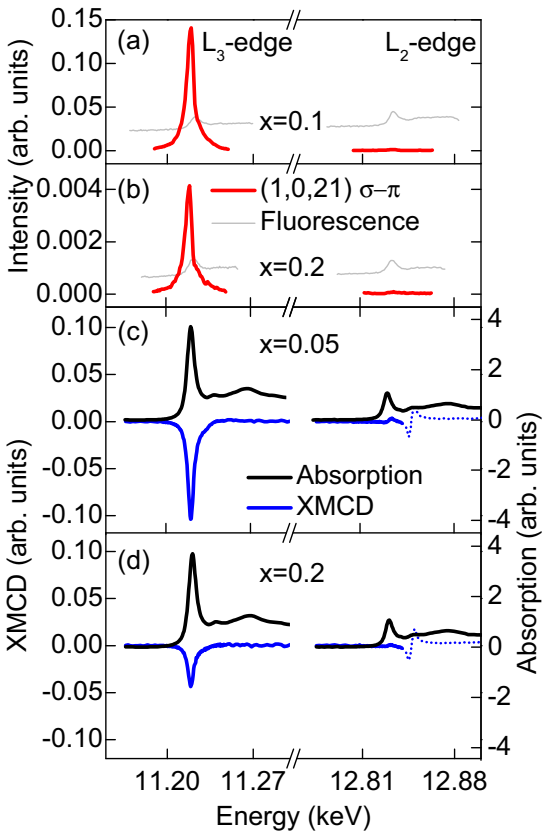

FIG. 8. (Color online) (a),(b) Energy scans through the iridium L_2 and L_3 edges using RMXS on $Sr_2Ir_{0.9}Ru_{0.1}O_4$ and $Sr_2Ir_{0.8}Ru_{0.2}O_4$ single crystals within the magnetically ordered phase ($T = 5$ K). The red solid lines correspond to RMXS with polarization of σ-π. The grey line, a fluorescence measurement, is performed to indicate the energy of the resonant L edges only and has been scaled to fit on the plot. (c),(d) XMCD and x-ray-absorption energy scans in a ± 3 T field at 1.8 K for $Sr_2Ir_{0.95}Ru_{0.05}O_4$ and $Sr_2Ir_{0.8}Ru_{0.2}O_4$. The variation of the XMCD signal above 12.84 keV (dotted line) is an artifact of the optics rather than from any XMCD signal from the sample.

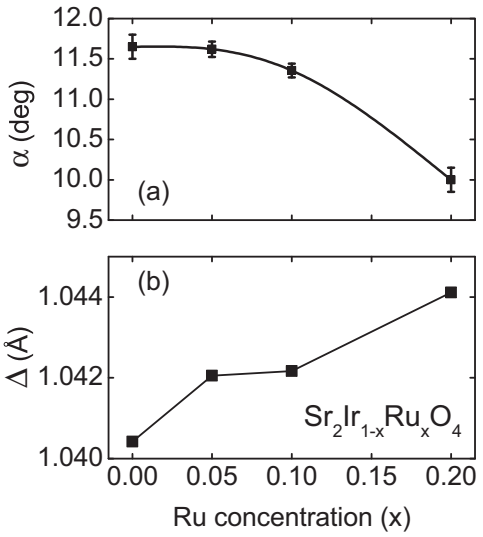

FIG. 9. Single-crystal neutron diffraction on $Sr_2Ir_{1-x}Ru_xO_4$ for $x = 0$, 0.05, 0.1, and 0.2 at 50 K. (a) The octahedral rotation in the ab plane (α). (b) Tetragonal distortion of the octahedra due to the difference between Ir-O bonds in the ab plane and along the c axis ($\Delta_{\text{Ir-O}}$).

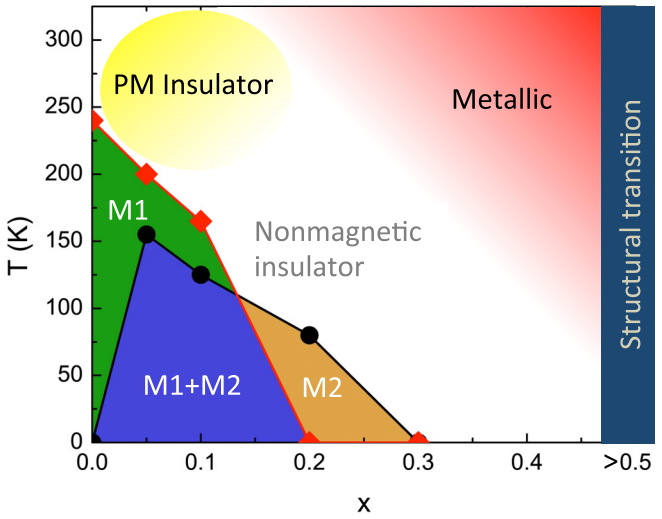

FIG. 10. (Color online) Phase diagram for $Sr_2Ir_{1-x}Ru_xO_4$. The data points correspond to transition temperatures from single-crystal neutron diffraction and RMXS. M1 denotes ab-plane magnetic ordering and M2 indicates c-axis ordering. The insulating regions are based on results presented in Ref. [15].

aligned AFM structure without an alteration of the $J_{\text{eff}} = 1/2$ state. The evolution of the octahedra is at least qualitatively in line with this behavior. However, the value of c/a predicted in Ref. [30] was 1.09 and therefore appreciably higher than the $\Delta_{\text{Ir-O}}$ value for even 20% doping. Therefore a structural route cannot be the sole reason for the observed spin flop.

F. Phase diagram of $Sr_2Ir_{1-x}Ru_xO_4$

Combining our neutron, x-ray, and magnetization results allows us to construct a phase diagram for the series $Sr_2Ir_{1-x}Ru_xO_4$ before the structural phase transition at $x > 0.5$; see Fig. 10. Starting from the undoped $x = 0$ insulator that undergoes magnetic order at 240 K the substitution of Ir^{4+} for Ru^{4+} leads to both a suppression of the metal-insulator transition and an evolution of the magnetic structure. The $x = 0$ magnetic structure (M1) is maintained up to $x = 0.1$, a larger value than previous dopings with Mn or Rh [17,20]. However, a coexistence at low temperature between the $x = 0$ basal plane ordering (M1) and the c-axis aligned magnetic structure (M2) exists for $x = 0.05$ and $x = 0.1$. Finally for $x = 0.2$ only the M2 ordering is present, before the final removal of long-range magnetic order at $x < 0.3$.

IV. DISCUSSION

The evolution and coexistence of long-ranged magnetically ordered structures in the series $Sr_2Ir_{1-x}Ru_xO_4$ is not observed in the limited previous studies of doped Sr_2IrO_4. This indicates the sensitivity and potential tuneabilty of Sr_2IrO_4 to a variety of perturbations. For Mn-doped Sr_2IrO_4 the magnetic structure is the same as the M2 phase discussed here with no region of the M1 structure [20]. For Rh-doped Sr_2IrO_4 the magnetic structure consists of spins in the ab plane [17], as found for Sr_2IrO_4 in a small applied field [4]. For the case of Rh-doped Sr_2IrO_4 there is no spin flop and there exists a small region of short-range correlations before the long-range basal plane magnetic ordering sets in. We find no such regions in our investigations of $Sr_2Ir_{1-x}Ru_xO_4$.

To explain the coexistence of magnetic structures in $Sr_2Ir_{1-x}Ru_xO_4$ we considered and ruled out chemical phase separation, both in terms of structural phase separation and mixed valence. Moreover while the similarities to the ortho-G-AF phase from Kugel-Khomskii orbital ordering in Ref. [26] is intriguing it remains unclear as to the validity of this model in $Sr_2Ir_{1-x}Ru_xO_4$. Instead we find electronic phase separation to be the most consistent scenario for the coexistence of M1 and M2 based on our results and in analogy to separate investigations [16,17,25]. One potential cause of this phase separation, that manifests in coexisting magnetic structures, is a competing and delicate balance of magnetic interactions in the $Sr_2Ir_{1-x}Ru_xO_4$ system due to altered exchange pathways. For example some bonds contain Ir-O-Ru-O-Ir bonds and others will contain Ir-O-Ir-O-Ir bonds that have different exchange interactions, extended to three dimensions. Since the correlation lengths of the two phases are not distinct then the phase separation is not limited to isolated small regions in the vicinity of the Ru dopant, but extends throughout the lattice. While the specific microscopic route to the spin-flop transition is puzzling, the alteration of the octahedra along with an introduction of anisotropy due to the dopant likely play a role. Despite the evolution and coexistence of magnetic structures the mechanism of the insulating state appears to remain unchanged and driven by the Mott mechanism splitting of the SOC enhanced $J_{\text{eff}} = 1/2$ ground state.

Our results show that the Ir moments remain long-range ordered up until Ru = 0.3. The alternative doping of Rh in the series $Sr_2Ir_{1-x}Rh_xO_4$ instead found a removal of magnetic order at around half the concentration of Rh = 0.17 [17]. They considered a percolation driven suppression of magnetic order,

in analogy to the cuprates, to most adequately describe the behavior. The large discrepancy between the concentration that magnetic order is suppressed between Rh and Ru doping at first glance appears to imply a divergence of behavior. However since the Rh introduced into Sr_2IrO_4 adopted the Rh^{3+} valance it did not simply replace the Ir^{4+} ions, but created two nonmagnetic dopants (Rh^{3+} and Ir^{5+}). Therefore that created an effective percolation value of $2x = 0.34$, that is close to the value we find for $Sr_2Ir_{1-x}Ru_xO_4$. Standard percolation theory predicts a value of $x = 0.4$ as the concentration for the removal of magnetic order. So while the behavior for both Ru- and Rh-doped Sr_2IrO_4 is consistent with a percolation scenario, it appears to fall short of a full description. A full understanding incorporating further interactions such as SOC, $4d$-$5d$ magnetic interactions, and band hybridization appears necessary to reproduce the observed behavior, with Ru doping potentially more favorable due to the direct replacement of Ir^{4+} with Ru^{4+} ions.

V. CONCLUSION

We have investigated the series $Sr_2Ir_{1-x}Ru_xO_4$ using both neutrons and resonant x-ray scattering to find the magnetic structure in the ordered regime of the phase diagram and assign the nature of the insulating state. Our results indicate a coexistence of two doping induced magnetic structures up to 10% Ru substitution, compatible with an electronic phase separated system. At higher Ru concentration of 20% the magnetic structure consists solely of c-axis aligned spins, indicating a spin-flop transition from the undoped Sr_2IrO_4 basal plane magnetic structure. Substituting 30% Ru removes long-range magnetic order. We are able to use the resonant x-ray L edges to assign the insulating behavior within the full magnetically ordered region of the phase diagram as consisting of a $J_{\text{eff}} = 1/2$ SOC enhanced insulating state.

ACKNOWLEDGMENTS

S.C. thanks A. M. Oles for illuminating discussions. This research at ORNL's High Flux Isotope Reactor was sponsored by the Scientific User Facilities Division, Office of Basic Energy Sciences, U.S. Department of Energy. Part of the work (A.F.M., C.C., D.M., B.C.S., G.C.) was supported by the U.S. Department of Energy, Office of Science, Basic Energy Sciences, Materials Sciences and Engineering Division. Use of the Advanced Photon Source, an Office of Science User Facility operated for the U.S. DOE Office of Science by Argonne National Laboratory, was supported by the U.S. DOE under Contract No. DE-AC02-06CH11357. This manuscript has been authored by UT-Battelle, LLC under Contract No. DE-AC05-00OR22725 with the U.S. Department of Energy. The United States Government retains and the publisher, by accepting the article for publication, acknowledges that the United States Government retains a non-exclusive, paid-up, irrevocable, world-wide license to publish or reproduce the published form of this manuscript, or allow others to do so, for United States Government purposes. The Department of Energy will provide public access to these results of federally sponsored research in accordance with the DOE Public Access Plan (http://energy.gov/downloads/doe-public-access-plan).

[1] W. Witczak-Krempa, G. Chen, Y. B. Kim, and L. Balents, Annu. Rev. Condens. Matter Phys. **5**, 57 (2014).
[2] X. Wan, A. M. Turner, A. Vishwanath, and S. Y. Savrasov, Phys. Rev. B **83**, 205101 (2011).
[3] D. Pesin and L. Balents, Nat. Phys. **6**, 376 (2010).
[4] B. J. Kim, H. Ohsumi, T. Komesu, S. Sakai, T. Morita, H. Takagi, and T. Arima, Science **323**, 1329 (2009).
[5] J. W. Kim, Y. Choi, J. Kim, J. F. Mitchell, G. Jackeli, M. Daghofer, J. van den Brink, G. Khaliullin, and B. J. Kim, Phys. Rev. Lett. **109**, 037204 (2012).
[6] S. Calder, G.-X. Cao, S. Okamoto, J. W. Kim, V. R. Cooper, Z. Gai, B. C. Sales, M. D. Lumsden, D. Mandrus, and A. D. Christianson, Phys. Rev. B **89**, 081104 (2014).
[7] G. Cao, A. Subedi, S. Calder, J.-Q. Yan, J. Yi, Z. Gai, L. Poudel, D. J. Singh, M. D. Lumsden, A. D. Christianson, B. C. Sales, and D. Mandrus, Phys. Rev. B **87**, 155136 (2013).
[8] S. Boseggia, R. Springell, H. C. Walker, H. M. Rønnow, C. Rüegg, H. Okabe, M. Isobe, R. S. Perry, S. P. Collins, and D. F. McMorrow, Phys. Rev. Lett. **110**, 117207 (2013).
[9] R. Dally, T. Hogan, A. Amato, H. Luetkens, C. Baines, J. Rodriguez-Rivera, M. J. Graf, and S. D. Wilson, Phys. Rev. Lett. **113**, 247601 (2014).
[10] F. Wang and T. Senthil, Phys. Rev. Lett. **106**, 136402 (2011).
[11] J. Kim, D. Casa, M. H. Upton, T. Gog, Y.-J. Kim, J. F. Mitchell, M. van Veenendaal, M. Daghofer, J. van den Brink, G. Khaliullin, and B. J. Kim, Phys. Rev. Lett. **108**, 177003 (2012).
[12] G. Jackeli and G. Khaliullin, Phys. Rev. Lett. **102**, 017205 (2009).
[13] Y. Maeno, H. Hashimoto, K. Yoshida, S. Nishizaki, T. Fujita, J. G. Bednorz, and F. Lichtenberg, Nature (London) **372**, 532 (1994).
[14] D. H. Torchinsky, H. Chu, L. Zhao, N. B. Perkins, Y. Sizyuk, T. Qi, G. Cao, and D. Hsieh, Phys. Rev. Lett. **114**, 096404 (2015).
[15] R. J. Cava, B. Batlogg, K. Kiyono, H. Takagi, J. J. Krajewski, W. F. Peck, L. W. Rupp, and C. H. Chen, Phys. Rev. B **49**, 11890 (1994).
[16] A. Glamazda, W.-J. Lee, K.-Y. Choi, P. Lemmens, H. Y. Choi, N. Lee, and Y. J. Choi, Phys. Rev. B **89**, 104406 (2014).
[17] J. P. Clancy, A. Lupascu, H. Gretarsson, Z. Islam, Y. F. Hu, D. Casa, C. S. Nelson, S. C. LaMarra, G. Cao, and Y.-J. Kim, Phys. Rev. B **89**, 054409 (2014).
[18] F. Ye, S. Chi, B. C. Chakoumakos, J. A. Fernandez-Baca, T. Qi, and G. Cao, Phys. Rev. B **87**, 140406 (2013).
[19] C. Dhital, T. Hogan, Z. Yamani, C. de la Cruz, X. Chen, S. Khadka, Z. Ren, and S. D. Wilson, Phys. Rev. B **87**, 144405 (2013).
[20] S. Calder, G.-X. Cao, M. D. Lumsden, J. W. Kim, Z. Gai, B. C. Sales, D. Mandrus, and A. D. Christianson, Phys. Rev. B **86**, 220403 (2012).
[21] In a 10% doped sample a single Ir column will contain a number of Ru atoms equal to 0.1 × number of Ir atoms per

column, which in our case is in the range 15–30, yielding a variation in the Ir column intensity of only 0.67%. This variation is much smaller than the standard deviation of the maxima in the line profile of Fig. 5(g), which is on the order of 5% and consistent with local variations in thickness of ± one Ir atom per column. This means that the variation in atomic column intensity due to 10% Ru doping is completely masked by local column thickness variations, and if the Ru atoms are randomly distributed we expect similar variations in Ir column intensity for the undoped and doped sample, as we observe.

[22] R. F. Egerton, *Electron Energy-Loss Spectroscopy in the Electron Microscope*, 2nd ed. (Plenum, New York, 1996).

[23] A. Zheludev, ResLib-3-axis RESolution LIBrary for MatLab.

[24] K. Kobayashi, T. Nagao, and M. Ito, Acta Crystallogr. Sect. A: Found. Crystallogr. **67**, 473 (2011).

[25] C. Dhital, T. Hogan, W. Zhou, X. Chen, Z. Ren, M. Pokharel, Y. Okada, M. Heine, W. Tian, Z. Yamani, C. Opeil, J. S. Helton, J. W. Lynn, Z. Wang, V. Madhavan, and S. D. Wilson, Nat. Commun. **5**, 3377 (2014).

[26] W. Brzezicki, J. Dziarmaga, and A. M. Oleś, Phys. Rev. B **87**, 064407 (2013).

[27] M. Moretti Sala, S. Boseggia, D. F. McMorrow, and G. Monaco, Phys. Rev. Lett. **112**, 026403 (2014).

[28] J. P. Clancy, N. Chen, C. Y. Kim, W. F. Chen, K. W. Plumb, B. C. Jeon, T. W. Noh, and Y.-J. Kim, Phys. Rev. B **86**, 195131 (2012).

[29] S. Boseggia, H. C. Walker, J. Vale, R. Springell, Z. Feng, R. S. Perry, M. M. Sala, H. M. Rønnow, S. P. Collins, and D. F. McMorrow, J. Physics: Condens. Matter **25**, 422202 (2013).

[30] P. Liu, S. Khmelevskyi, B. Kim, M. Marsman, D. Li, X.-Q. Chen, D. D. Sarma, G. Kresse, and C. Franchini, Phys. Rev. B **92**, 054428 (2015).